Full Wave Analysis of Microwave Monolithic Circuit Devices Using a Generalized Yee-Algorithm Based on an Unstructured Grid

Stephen D. Gedney, Faiza S. Lansing, and Daniel L. Rascoe

Abstract— **A generalized Yee-algorithm is presented for the temporal full-wave analysis of microwave monolithic integrated circuit (MMIC) devices. This algorithm has the significant advantage over the traditional Yee-algorithm in that it is based on unstructured and irregular grids. Thus, using the generalized Yee-algorithm, MMIC devices that contain curved conductors or complex geometries can be more accurately and conveniently modeled using standard automatic grid generation techniques. The generalized Yee-algorithm is based on the time-marching solution of the discrete form of Maxwell's equations in their integral form. A correction scheme is introduced that is stable, maintains second-order accuracy, and maintains the divergenceless nature of the flux densities. Furthermore, by structuring the algorithm as a series of sparse matrix-vector multiplications, the generalized Yee-algorithm can be efficiently implemented on vector or parallel high performance computers.**

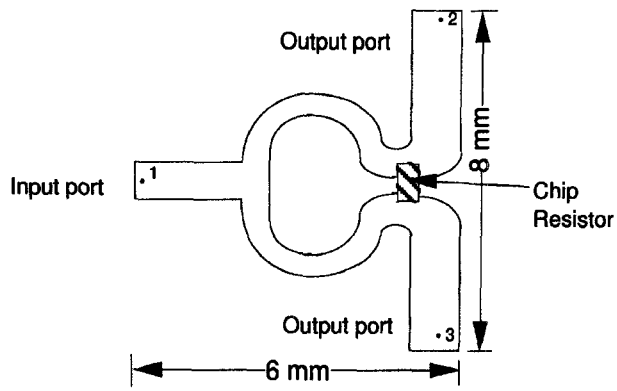

Fig. 1. Wilkinson power divider at ka-band (32 GHz).

I. Introduction

TRADITIONALLY, microwave monolithic integrated circuits (MMIC's) have been analyzed using approximate techniques based on planar circuit concepts and transmission line models. While these models do provide very accurate analysis of MMIC's at lower frequencies, at higher frequencies such methods do not accurately account for the increasingly significant affects of field fringing, coupling, nonlinearities and radiation. In order to fully account for these phenomena, a full wave analysis becomes necessary.

The finite-difference time-domain (FDTD) method, based on the traditional Yee-algorithm [1], has been successfully applied to the analysis of both active and passive planar microstrip circuits and MMIC's [2]–[5]. The FDTD method is highly efficient and very well suited for many problems of interest, however, it has some significant limitations. Curved structures, such as the power divider illustrated in Fig. 1, must be modeled using a staircase-type approximation. To reduce the discretization error associated with such approximations, the mesh must be highly refined. Furthermore, modeling must often be done manually. These issues have motivated the development of new techniques based on non orthogonal and unstructured grids [6–9]. Earlier work [6], [7] expressed the FDTD in curvilinear coordinates. A more robust technique introduced by J.-F. Lee, [8], [9], assumes a locally curvilinear coordinate system for each cell of an irregular structured grid. This is efficiently accomplished by introducing the local covariant and contravariant projections associated with each grid cell approximating each grid cell as a parallelepiped.

Unfortunately, none of the above treatments can be applied to a general unstructured grid. Other methods to treat more general grid structures have recently been introduced. In [10], Rappaport and Smith use a grid based on triangular pyramids. Second-order accuracy can be exactly maintained providing the interior angles of the triangular faces are 60° and the rectangular faces are orthogonal to the triangular faces. In [11], Holland introduced another technique for treating more general grid structures. They demonstrated a method in two-dimensions (2–D) based on a local expansion of the field into an orthogonal basis.

More generalized techniques were recently presented by Madsen and Ziolkowski in [12] and by Madsen in [13]. In [13] Madsen addresses a technique based on unstructured grids, and seeks a correction scheme with second-order accuracy despite the grid irregularity. The stability of the solution after very large number of time iterations is found to be highly dependent upon the accuracy of the correction scheme. In [13], Madsen presents a correction scheme, which projects the normal fields

Manuscript received July 19, 1993; revised April 19, 1996. This work was supported in part under JPL/NASA Contract 959534 with the University of Kentucky, ARO Grant #DAHO4-94-G-0243, 32-node Intel iPSC/860 funded under NSF grant EMS-9206014, Army Research Office Grant #DAAHO4-93-G-0453, and CEM grant iSC022 492 awarded through the Intel Supercomputer Systems Division.

S. D. Gedney is with the Department of Electrical Engineering, University of Kentucky, Lexington, KY 40506-0046 USA.

F. S. Lansing and D. L. Rascoe are with the Spacecraft Telecommunications Equipment Section, Jet Propulsion Laboratory, California Institute of Technology, Pasadena, CA 91109 USA.

Publisher Item Identifier S 0018-9480(96)05654-2.

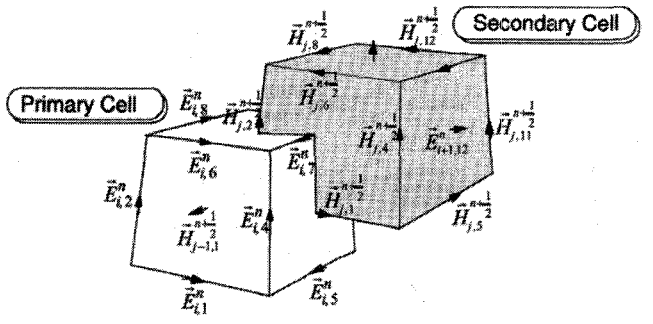

Fig. 2. Unstructured dual grid cells.

onto the grid edges, maintains second-order accuracy and is numerically stable.

Influenced by the recent work of Madsen [13], an efficient means has been developed for treating the three-dimensional (3-D) problem based on unstructured grids that provides a second-order accurate solution. This algorithm is referred to here as the generalized Yee-algorithm [14]. Madsen's correction scheme in [13] is used to project the normal fields onto the grid edges, yet, it is implemented such that the memory requirements for the correction term are reduced, while still maintaining the divergenceless nature of the approximate field. The algorithm treats the time stepping iterations of the generalized Yee-algorithm as a series of matrix-vector multiplications, leading to an efficient algorithm that is vectorizable and has a high degree of parallelism.

In this paper, the development of the generalized Yee-algorithm is introduced in Section II, modeling lumped loads directly with Maxwell's equations is discussed in Section III, the computationally efficient implementation of the generalized Yee-algorithm is discussed in Section IV, and some numerical examples based on this method are described in Section V.

II. Generalized Yee-Algorithm

The generalized Yee-algorithm is based on a direct solution of Maxwell's equations in their integral form within a closed 3-D volume. The electric and magnetic fields are discretized over a dual grid structure formed by a primary and secondary grid, as illustrated in Fig. 2. The primary grid is composed of general fitted polyhedra distributed throughout the volume. The secondary grid (or dual grid) is built up of the closed polyhedra whose edges connect the centroids of adjacent primary cells, penetrating shared faces. Fig. 2 illustrates adjoining primary and secondary grid cells that are hexahedron. Along each edge of the primary grid cells, an electric field vector is defined. Similarly, a magnetic field vector is located along each secondary grid cell edge.

Faraday's Law and Ampre's Law are approximated by discretizing the surface and line integrals over each primary grid cell face and secondary grid cell faces, respectively. The fields are assumed to be constant over their respective faces and along each edge. The time derivative is then approximated using a central difference approximation. This leads to the discrete form of Faraday's and Ampre's Laws, respectively

$$\left(\vec{B}_i^{n+1/2} - \vec{B}_i^{n-1/2}\right) \cdot \hat{n}_p \left(\frac{A_i}{\Delta t}\right) = -\sum_{j=1}^{N_{e_i}} \vec{p}_j \cdot \vec{E}_{i,j}^{n} \tag{1a}$$

$$(\vec{D}_i^{n+1} - \vec{D}_i^{n}) \cdot \hat{n}_s \left(\frac{A_i}{\Delta t}\right) + (\vec{D}_i^{n+1} + \vec{D}_i^{n}) \cdot \hat{n}_s \left(\frac{\sigma_{\text{ave}}}{2\varepsilon_{\text{ave}}} A_i\right) + \vec{J}_i^{n+1/2} \cdot \hat{n}_s A_i = \sum_{j=1}^{N_{e_i}} \vec{s}_j \cdot \vec{H}_{i,j}^{n+1/2} \tag{1b}$$

where the superscripts indicate the time index, N_{e_i} is the number of edges bounding the i-th face of the primary grid [in (1a)] or the secondary grid [in (1b)], A_i is the area of the i-th face, $\hat{n}_p$ and $\hat{n}_s$ are the unit normals to the primary and secondary grid faces, respectively, $\vec{p}_j$ and $\vec{s}_j$ are the length vectors of the j-th edges bounding the primary and secondary grid faces, respectively, and ε_{ave} and σ_{ave} are derived in Appendix A.

The field solution is obtained from (1a) and (1b) resulting in the explicit time stepping algorithm

$$\vec{B}_i^{n+1/2} \cdot \hat{n}_p = \vec{B}_i^{n-1/2} \cdot \hat{n}_p - \left(\frac{\Delta t}{A_i}\right) \sum_{j=1}^{N_{e_i}} \vec{p}_j \cdot \vec{E}_{i,j}^{n} \tag{2a}$$

$$\vec{D}_i^{n+1} \cdot \hat{n}_s = \left(\frac{1}{\frac{1}{\Delta t} + \frac{\sigma_{\text{ave}}}{2\varepsilon_{\text{ave}}}}\right) \left\{ \left(\frac{1}{\Delta t} - \frac{\sigma_{\text{ave}}}{2\varepsilon_{\text{ave}}}\right) \vec{D}_i^{n} \cdot \hat{n}_s + \vec{J}_i^{n+1/2} \cdot \hat{n}_s + \frac{1}{A_i} \sum_{j=1}^{N_{e_i}} \vec{s}_j \cdot \vec{H}_{i,j}^{n+1/2} \right\}. \tag{2b}$$

If the fields are discretized over a regular orthogonal rectangular grid, (2a) and (2b) reduce to the traditional Yee-algorithm. For general unstructured grids, (2a) and (2b) provide a more general approximation for the fields. However, before proceeding, it is recognized that for a general unstructured and non orthogonal grid, it cannot be said that $\hat{n}_p = \hat{s}$ or $\hat{n}_s = \hat{p}$. More specifically, the magnetic flux density normal to the primary grid face is updated in (2a). However, the update of the electric flux density in (2b) requires the projection of the magnetic field onto a dual edge. Since it cannot be assumed that $\hat{n}_p = \hat{s}$, the normal field must be projected onto the complimentary grid edge. Since the normal field alone cannot uniquely describe the edge component, a secondary expression must be introduced to perform the projection.

To uniquely project the magnetic field onto the secondary grid edge it is necessary to perform an interpolation of the magnetic flux densities normal to local adjacent faces. This must be done such that: 1) the flux projected onto the edges must also be divergenceless in charge free medium, and 2) the time stepping algorithm must maintain stability. To this end, a correction scheme similar to Madsen's in [13] which meets these criterion is used here. The most significant difference between the current approach and Madsen's approach is that Madsen interpolates the time rate of change of the flux density, whereas, here the flux density is interpolated. This leads to an

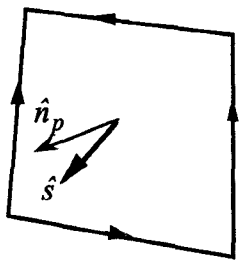

Fig. 3. Primary grid face with normal vector $\hat{n}_p$ penetrated by dual edge directed along the unit vector $\hat{s}$.

efficient computational implementation of the algorithm, as discussed in Section IV.

Assume that each face is shared by N_c cells (where $N_c = 2$ or 1). Each face is also assumed to be bound by N_e edges which connect N_e vertices. Referring to Fig. 4, assume that the i-th vertex is shared by three faces of the j-th cell. Equation (2a) is used to update the normal magnetic flux densities passing through each face. Then, the magnetic flux density associated with the i-th vertex and the j-th cell can be computed by solving the 3 × 3 system of equations

$$\begin{aligned} \vec{B}_{i,j} \cdot \vec{N}_P &= \vec{B} \cdot \vec{N}_P \\ \vec{B}_{i,j} \vec{N}_{P_{i,j}} &= \vec{B} \cdot \vec{N}_{P_{i,j}} \\ \vec{B}_{i,j} \cdot \vec{N}_{P_{i+1,j}} &= \vec{B} \cdot \vec{N}_{P_{i+1,j}} \end{aligned} \tag{3}$$

where the $\vec{N}_P$ are the area vectors normal to each primary grid face. Since the right-hand-side is known from (2a), (3) is used to solve for the three orthogonal components of $\vec{B}_{i,j}$. Subsequently, this is performed for each of the vertices of the face ($i = 1, N_e$) and for each cell ($j = 1, N_c$) shared by the face. At this point it is noted that $\vec{B}_{i,j}$ is not an interpolation for the total field, but rather a local value associated with the i,j-th corner shared by the face. The magnetic flux density vector over the face is then expressed by the interpolation

$$\vec{B} = \frac{\sum_{j=1}^{N_c} \sum_{i=1}^{N_e} |w_{i,j}| \vec{B}_{i,j}}{\sum_{j=1}^{N_c} \sum_{i=1}^{N_e} |w_{i,j}|} \tag{4}$$

where the weighting factors are computed by the triple scalar product

$$w_{i,j} = \vec{N}_P \cdot (\vec{N}_{P_{i,j}} \times \vec{N}_{P_{i+1,j}}). \tag{5}$$

Finally, given the magnetic flux density in (4), it can be uniquely projected onto the secondary cell edge via the dot product $\vec{B} \cdot \hat{s}$.

It can be shown that the interpolated $\vec{B}$ in (4) satisfies Gauss's Law in discrete form. To this end, consider the magnetic flux density at the current and the previous time steps. Then

$$\frac{\left[\int_V \nabla \cdot \vec{B}^{n+1.2}\, dV - \int_V \nabla \cdot \vec{B}^{n-1/2}\, dV\right]}{\Delta t}$$

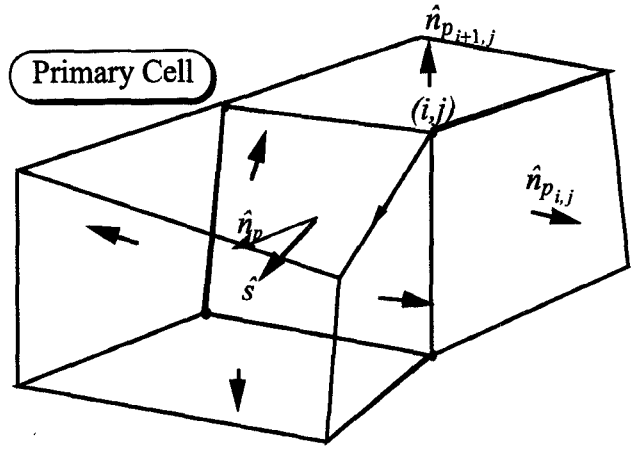

Fig. 4. Adjacent primary grid cells sharing common face with magnetic fields normal to each face known.

$$= \int_V \nabla \cdot \frac{\partial \vec{B}^n}{\partial t}\, dV \tag{6}$$

where V is the volume of the primary cell. From Stoke's theorem and Faraday's law, the right-hand-side of (6) is expressed as

$$\begin{aligned} \int_V \nabla \cdot \frac{\partial \vec{B}^n}{\partial t}\, dV &= \oiint_S \frac{\partial \vec{B}^n}{\partial t} \cdot d\vec{s} = \sum_{i=1}^{N_f} \int_{S_i} \frac{\partial \vec{B}^n}{\partial t} \cdot d\vec{s}_i \\ &= -\sum_{i=1}^{N_f} \oint_{C_i} \vec{E}^n \cdot d\vec{\ell} = 0 \end{aligned} \tag{7}$$

where, S is the surface bounding the cell volume V, S_i is the i-th face of the cell, and C_i is the contour bounding S_i. The expression is zero since the edges of the cell are traversed twice in opposing directions when evaluating the line integral. Since this is true for each $\vec{B}$ the argument can be extended for the $\vec{B}$ appearing in (4). Finally, assuming that the initial value of $\vec{B}$ is divergenceless throughout the volume, then from (6) and (7), it can be stated that

$$\oiint_S \vec{B}^{n+1/2} \cdot d\vec{s} = 0. \tag{8}$$

By duality, the displacement flux density is projected onto the primary grid edges using

$$\vec{D} \cdot \hat{p} = \frac{\sum_{j=1}^{N_c} \sum_{i=1}^{N_e} |w_{i,j}| \vec{D}_{i,j}}{\sum_{j=1}^{N_c} \sum_{i=1}^{N_e} |w_{i,j}|} \cdot \hat{p}. \tag{9}$$

It can be shown that the displacement flux density in (9) also satisfies the discrete form of Gauss's Law. Finally, the field updates can be performed by computing the vector fields normal to the primary or secondary grid faces using (2a) or (2b), then project them onto the edges of the secondary or primary grids using (4) or (9), respectively. By introducing the correction terms in (4) and (9) it can be shown that second-order accuracy of the algorithm is maintained, assuming that

the time increment Δt satisfies the Courant stability criterion. The exact stability criterion would require an eigenvalue analysis of the combined update expressions in (2a), (2b), (4) and (9) in [8]. Unfortunately, this will be problem dependent due to the unstructured nature of the grid. Through numerical experimentation, however, a relationship has been established which provides an excellent estimate of the stability criterion for tetrahedral, pentahedral and hexahedral elements

$$\Delta t < \frac{1}{c \sup \left[\sum_{i=1}^{3} \frac{1}{\ell_i^2} \right]} \tag{10}$$

where, c is the speed of light, and the $\ell_i (i = 1, 3)$ are three edges in each cell sharing a common vertex. This expression provides an accurate estimate for the time step that is in general within 10% of the actual stability criterion. It is observed from (10) that the time step will be bound by the smallest edge length in the model.

The greatest strength of the above technique is that it is based on general, unstructured grids, and thus can be applied to problems with complex 3-D geometries. Furthermore, this method is well suited for the large variety of commercially available automatic numerical grid generation software packages for modeling and meshing the geometry. One disadvantage, however, is that since the grid is unstructured and irregular, the numerical grid must be stored (this is not required for the regular grid-based FDTD method). Second, it would appear that either a significant number of floating point operations will be required during each time iteration (e.g., to compute the area of each face, the unit normals, the edge vectors, the weighting factors, etc.), or much more memory will be needed to store most of these parameters. In Section IV, techniques are introduced that minimizes both the floating point operations and vastly reduces the memory requirements of the generalized Yee-algorithm.

III. Lumped Loads

To accurately model hybrid and integrated planar microwave circuits, it is necessary to include lumped circuit elements. Using general voltage-current relationships of lumped circuit elements it is possible to model the interaction of the fields with lumped circuits directly with Maxwell's equations.

From the generalized current concept [15], Ampere's Law is expressed as

$$\oint_C \vec{H} \cdot d\vec{\ell} = I + I_d + I_c + I_l \tag{11}$$

where I_d is the displacement current, I_c is the conduction current, and I_l is the lumped current through the lumped element. The voltage along any primary grid edge of the model will be locally approximated by the line integral of the electric field along the edge. If the electric field is known at the present time step, then the lumped current along the edge can be simply expressed through the voltage-current relationship of the lumped element

$$I_l = f(V_{12}) = f\left(\int_{P_1}^{P_2} \vec{E} \cdot d\vec{\ell} \right). \tag{12}$$

Consider the linear, passive elements R_l (resistor), C_l (capacitor), and L_l (inductor). If each of these were placed along a primary grid edge, the lumped current induced through these elements would be expressed as

$$\begin{aligned} I_{l_R}^{n+1/2} &= \frac{\vec{p} \cdot (\vec{E}^{n+1} + \vec{E}^{n})}{2R_l}, \\ I_{l_C}^{n+1/2} &= C_l \frac{\vec{p} \cdot (\vec{E}^{n+1} - \vec{E}^{n})}{\Delta t}, \\ I_{l_L}^{n+1/2} &= \sum_{j=0}^{n} \frac{\vec{p} \cdot (\vec{E}^{j+1} + \vec{E}^{j})}{2L_l} \Delta t. \end{aligned} \tag{13}$$

Based on this relationship, discrete elements can be directly incorporated into (2b), where, $I_l^{n+1/2} = A_i \vec{J}_i^{n+1/2} \cdot \hat{n}_s$ for the i-th edge.

IV. Enhancing Computational Efficiently

The generalized Yee-algorithm has the potential to be computationally expensive and memory intensive. However, if it is treated in the appropriate fashion, the algorithm can be employed very efficiently. To this end, the generalized Yee-algorithm can be thought of as a series of linear operations acting on the fields that are normal to the primary and the secondary grid faces. These linear operations can be expressed in their discrete form simply as matrix-vector multiplications. For example, consider (2a). The line integral can be expressed as a sparse matrix. The i-th row of the matrix has identically N_{e_i} nonzero column elements. Since all zero row elements have no contribution only the nonzero elements need be stored. Subsequently, (2a) can be expressed as

$$b_n = b_n - A_h A_{ec} d_n \tag{14}$$

where b_n is the vector of magnetic fluxes normal to each primary grid cell face, d_n is the vector of electric fluxes normal to the secondary grid faces, A_h is a sparse matrix representing the line integral in (2a), and A_{ec} is a sparse matrix of order representing the projection operation in (9). Similarly

$$d_n = D_e d_n - A_e A_{hc} b_n \tag{15}$$

where D_e is a diagonal matrix derived from the self term in (2b), A_e is a sparse matrix representing the line integral in (2b), and A_{hc} is a sparse matrix derived from the projection operator in (4).

The number of nonzero entries A_{hc} and A_{ec} will be dependent upon the number of faces used in the interpolation in (4) and (9), respectively. For example, from (4), there will be $N_c N_e + 1$ nonzero entries in each row of A_{hc}, where N_c and N_e are dependent upon the local mesh characteristics. Each row entry is then derived explicitly from (3)–(5). To this end, the left-hand side of (3) can be represented by a 3 × 3 matrix [A] times the vector unknown representing $\vec{B}_{i,j}$, where the three rows of [A] represent the x, y, and z components of

$\vec{N}_P, \vec{N}_{P_{i,j}}$, and $\vec{N}_{P_{i+1,j}}$, respectfully. Subsequently, the local interpolated field is then solved as

$$\begin{bmatrix} \vec{B}_{i,j} \cdot \hat{x} \\ \vec{B}_{i,j} \cdot \hat{y} \\ \vec{B}_{i,j} \cdot \hat{z} \end{bmatrix} = [A]^{-1} \begin{bmatrix} \vec{B} \cdot \vec{N}_P \\ \vec{B} \cdot \vec{N}_{P_{i,j}} \\ \vec{B} \cdot \vec{N}_{P_{i+1,j}} \end{bmatrix}. \tag{16}$$

Then, letting $[C] = [A]^{-1}$, and $\hat{s} = s_x\hat{x} + s_y\hat{y} + s_z\hat{z}$, it follows that

$$\begin{aligned} |w_{i,j}|\vec{B}_{i,j} \cdot \hat{s} = |w_{i,j}|\{&[c_{11}s_x + c_{21}s_y + c_{31}s_z]\vec{B} \cdot \vec{N}_P \\ &+ [c_{12}s_x + c_{22}s_y + c_{32}s_z]\vec{B} \cdot \vec{N}_{P_{i,j}} \\ &+ [c_{13}s_x + c_{23}s_y + c_{33}s_z]\vec{B} \cdot \vec{N}_{P_{i+1,j}}\} \end{aligned} \tag{17}$$

where the c_{ij} represent the elements of $[C]$. The entry in (17) weighting $\vec{B} \cdot \vec{N}_P$ will contribute to the diagonal term of A_{hc}, and the entries weighting $\vec{B} \cdot \vec{N}_{P_{i,j}}$ and $\vec{B} \cdot \vec{N}_{P_{i+1,j}}$ will contribute to the off diagonal terms. Then, summing over all i and j in (4), each row entry in A_{hc} can be assembled. It is noted that in any region where the grid is orthogonal , the off-diagonal elements of A_{hc} will be zero, and the diagonal term will be unity. This virtue can easily be exploited to conserve memory.

The sparse matrices in (13) and (14) need only be computed once and then stored using a compressed storage scheme. Subsequently, each time iteration consists of a set of matrix-vector multiplications, which are very computationally efficient and are easily parallelizable. A remaining issue is the efficient construction of these matrices. This is accomplished by constructing the matrices on a cell-by-cell basis. To this end, the secondary grid is never specifically constructed since there is sufficient information to construct the matrices A_e, A_h, D_e, A_{ec}, and A_{hc} from the primary grid cells alone. Subsequently, the matrices can be assembled by scanning through all the cells sequentially.

V. Numerical Examples

A computer program based on the generalized Yee-algorithm has been implemented on the 512-node Intel Delta Supercomputer located at the California Institute of Technology. It has also been implemented on an iPSC/860 hypercube, JPL's CRAY-YMP, an SGI Power Challenge and an HP workstation (note that porting the code to these other platforms only required changing the paths of I/O files). The program was interfaced with a commercial CAD software package (SDRC I-DEAS) to generate the circuit models and the primary grid. When the circuits are situated in unbounded regions, the discretization volume is truncated by planar boundaries. A second-order accurate absorbing boundary condition (ABC) based on the dispersive boundary condition [16] is used to update the fields on the truncation boundary walls, minimizing any nonphysical reflections (this results in < -40 dB reflection error across the entire bandwidth). It is noted that the mesh in the immediate vicinity of the exterior boundaries must be orthogonal for this ABC to be stable. This is done automatically by the software by extending an orthogonal mesh out from the initial unstructured mesh created by the automatic mesh generator. The mesh is then spatially

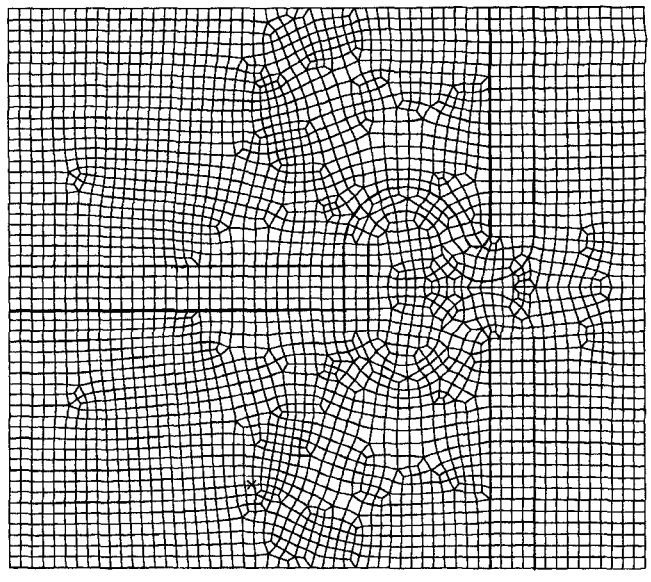

Fig. 5. Cross section of unstructured mesh used to discretize the Wilkinson power divider.

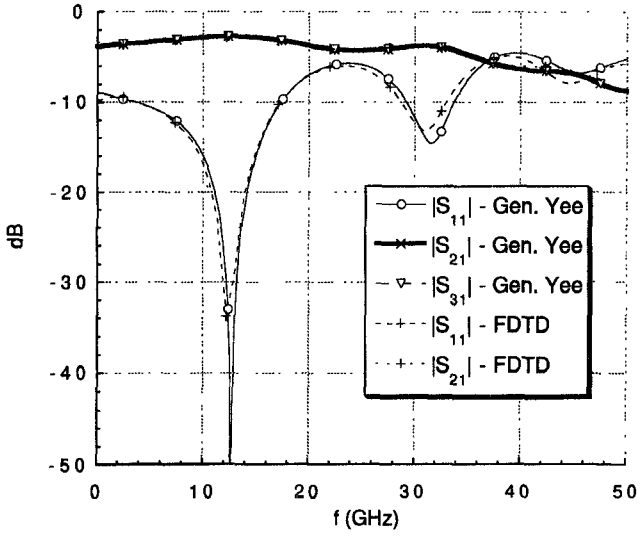

Fig. 6. S-parameters of Wilkinson power divider computed using the generalized Yee-algorithm using an unstructured grid and an FDTD algorithm using a regular orthogonal grid.

decomposed into contiguous subregions using the recursive inertia partitioning algorithm [17] (this decomposition is done in a manner that equally distributes the faces and edges of the primary grid among all subregions). Once the simulation is completed, one can extract data to compute the S-parameters, characteristic impedances and propagation constants. The computation of these parameters is done in the manner outlined in [2]. One can also visualize the interaction of the electric and magnetic fields in the device as a function of time. This alone has been extremely helpful to identify sources of radiated fields, coupling and resonances.

The computer program has been extensively validated through comparison with other numerical methods and published results. One such validation was the Wilkinson power divider illustrated in Fig. 1. The power divider is printed on a 15 mil TMM substrate ($\varepsilon_r = 3.25$). The input

TABLE I
CPU TIMES RECORDED ON AN iPSC/860 FOR THE GENERALIZED YEE-ALGORITHM WILKINSON POWER DIVIDER

Platform	1 Proc.	2 Proc.	4 Proc.	8 Proc.	16 Proc.	32 Proc.
Gen. Yee	2427 s	1285 s	674 s	373 s	225 s	137 s
FDTD	2275 s	1194 s	680 s	404 s	230 s	151 s

and output ports are 50 Ω (the strip width is 36 mil). For isolation, a 100 Ω chip resistor is placed across the apex of the power divider. This was modeled as a lumped load, as described in Section III. The input port was excited with a time varying Gaussian pulse with a bandwidth of 42 GHz. The volume enclosing the power divider was discretized using general hexahedron. A cross-section of the mesh in the plane of the microstrip line is illustrated in Fig. 5. A time step of 0.14 ps was used for the simulation, and required only 3000 time steps.

The first row of the scattering matrix of the Wilkinson power divider computed using the generalized Yee-algorithm is plotted versus frequency in Fig. 6. These results were obtained from a single time-domain simulation and an FFT was used to compute the frequency domain signals. The two output ports carry equal power, and are exactly in phase (not shown here). These results are compared with results obtained using a FDTD simulation based on an orthogonal regular lattice (details of this program are described in [18]).

The 3-D mesh modeling the Wilkinson power divider consisted of 65 824 hexahedron. This leads to roughly 412 200 degrees of freedom. The CPU times required to perform 3000 iterations on an iPSC/860 are recorded in Table I. These are also compared with the CPU times required by the FDTD algorithm. The FDTD lattice had a dimension of $107 \times 81 \times 23$, where $dx = dy = 0.114\,681$ mm, $dz = 0.063\,50$ mm, and $dt = 0.14$ ps. The FDTD algorithm was also executed for 3000 time iterations. For this small example, the FDTD algorithm and the generalized Yee algorithm have comparable CPU times. Interestingly, the generalized Yee algorithm has slightly better speedups as the number of processors is increase. This is due to the fact that as the problem size on each processor gets smaller, the CPU speed per processor decreases for the FDTD code as the vector lengths decrease [18]. On the other hand, due to indirect addressing, the generalized Yee algorithm is not as efficient on a pipelined processor, and the CPU speed per processor is fairly constant as the problem size decreases.

Fig. 7 illustrates a Gysel power divider (3 dB, in-phase). This divider is tuned to 34 GHz and is designed to be quite broad band. It is printed on a 10 mil Alumina substrate ($\varepsilon_r = 9.9$) and its ports are 50 Ω microstrip lines (a width of 9.9 mil). Isolation is provided by two 100 Ω branches that are terminated by a 50 Ω series resistance and a vertical connection to the ground plane. The first row of the scattering matrix over a broad band for this device using the generalized Yee-algorithm is illustrated in Fig. 8. The 3-D mesh modeling the Gysel power divider consisted of 353 980 hexahedron, leading to roughly 2 million degrees of freedom. The solution required time 8,000 iterations ($dt = 0.05$ ps) which required 2,272 CPU-sec to solve on 16 processors of an Intel iPSC/860

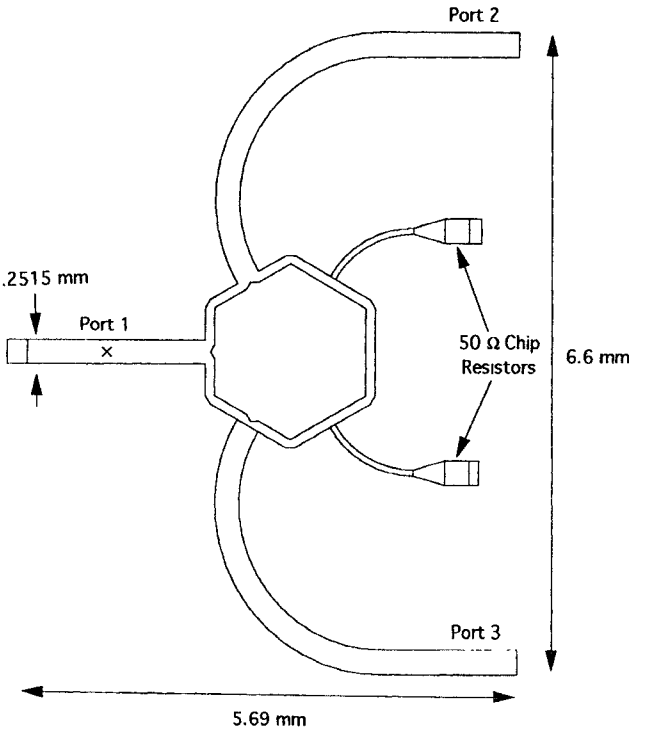

Fig. 7. Gysel power divider printed on a 10-mil Alumina substrate ($\varepsilon_r = 9.9$).

(1,256 CPU-sec on 32 processors). The results in Fig. 8 are also compared to those obtained using the FDTD method. The FDTD lattice had a dimension of $397 \times 253 \times 23$, where $dx = 0.023\,916\,5$ mm, $dy = 0.024\,716\,4$ mm, $dz = 0.042\,333\,33$ mm, and $dt = 0.05$ ps. This was the largest mesh size found that would provide an accurate model of the complex geometry using an orthogonal grid. The FDTD algorithm was also executed for 8,000 time iterations, and required 3,792 CPU-sec to solve on a 16 processor iPSC/860 (2,232 CPU-sec on 32 processors), which is roughly twice the CPU time as compared to the generalized Yee algorithm. Due to the regularity of the FDTD grid, the modeling task was also much more time consuming. Even though we have automated this task, it is still difficult to realize an accurate description of complex geometries, such as the Gysel power divider, using a regular orthogonal grid. Furthermore, to accurately model structures with highly detailed geometries, highly refined grids become necessary, which impacts the global grid size of the FDTD algorithm and subsequently the CPU time and memory requirements.

VI. SUMMARY

In this paper, the generalized Yee-algorithm has been presented. The algorithm is an explicit time-marching method

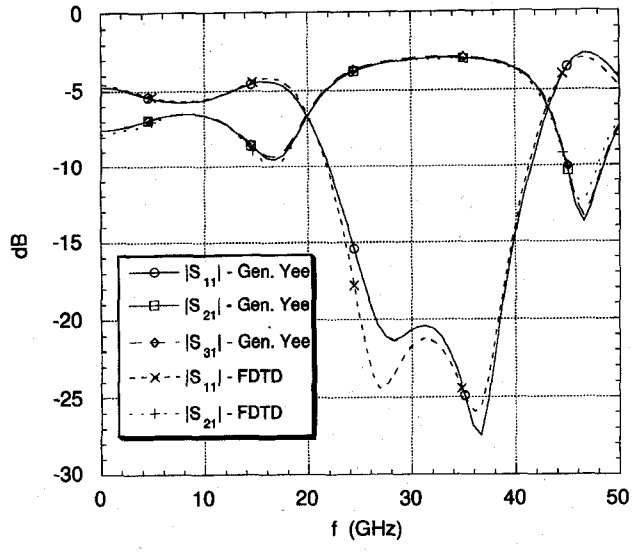

Fig. 8. S-parameters of Gysel power divider using the generalized Yee-algorithm.

based on the discretization of Maxwell's equations in their integral form using unstructured and irregular dual grids. This algorithm is much more robust than the traditional FDTD method in that it can be used to accurately model MMIC devices with much more general geometries. Furthermore, by treating the time-marching algorithm as a series of matrix vector multiplications, the algorithm is ideal for implementation on high performance parallel computers.

It is anticipated that the generalized Yee-algorithm will be a robust and computationally efficient tool for the analysis of microwave monolithic integrated circuits, and can readily exploit the scalable massively parallel high performance computers of the future for the solution of electrically large and dense MMIC devices.

APPENDIX A

In this Appendix, the average permittivity and conductivity of a secondary cell face is computed. Consider the face, defined as the surface S and bound by the contour C, of a secondary cell of an irregular and unstructured grid, e.g., Fig. 9. It is assumed that the edge passes through the centroid of the face and is tangential to the interface of boundary shared by the four materials $(\varepsilon_1,\sigma_1),(\varepsilon_2,\sigma_2),(\varepsilon_3,\sigma_3)$, and (ε_4,σ_4). In discrete form, Ampère's law is undefined since the permittivity of the face is ambiguous as referenced to the electric field passing through it's centroid. Subsequently, the surface of integration can be decomposed to four distinct surfaces, each with constant permittivity $\varepsilon_i (i = 1,2,3,4)$. Thus in discrete form, Ampère's law is expressed as

$$\sum_{i=1}^{4}\left(\frac{\partial}{\partial t}\iint_{S_i}\varepsilon_i\vec{E}\cdot d\vec{s}+\iint_{S_i}\sigma_i\vec{E}\cdot d\vec{s}\right)=\sum_{i=1}^{4}\oint_{C_i}\vec{H}\cdot d\vec{\ell} \tag{A1}$$

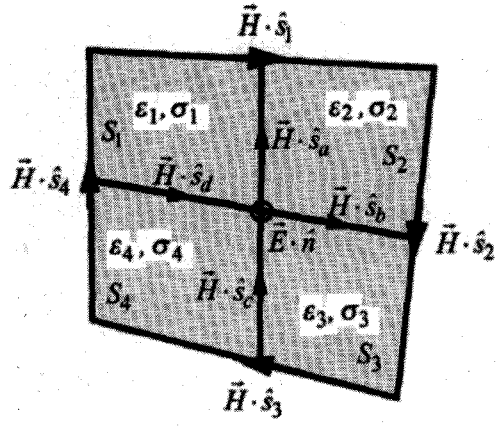

Fig. 9. Secondary cell face.

where, S_i is the surface of each subarea that is bound by the contour C_i. Over each S_i, we have

$$(\vec{E}_i^{n+1}-\vec{E}_i^{n})\cdot\hat{n}\left(\frac{\varepsilon_i}{\Delta t}A_i\right)+(\vec{E}_i^{n+1}+\vec{E}_i^{n})\cdot\hat{n}\left(\frac{\sigma_i}{2}A_i\right)=\sum_{j=1}^{N_{e_i}}\vec{\ell}_j\cdot\vec{H}_{i,j}^{n+1/2}. \tag{A2}$$

It is assumed that $\vec{E}_i^n\cdot\hat{n}$ in each subcell $(i=1,2,3,4)$ is tangential to the boundary interface, then it can be approximated that

$$\vec{E}_1^n\cdot\hat{n}\approx\vec{E}_2^n\cdot\hat{n}\approx\vec{E}_3^n\cdot\hat{n}\approx\vec{E}_4^n\cdot\hat{n}\approx\vec{E}^n\cdot\hat{n}. \tag{A3}$$

It is noted that this is in general a good approximation since the numerical grid is constructed such that the edge through the center of the secondary cell face must be tangential to the boundary surface. Subsequently, it is assumed that the edges extending above or below the boundary interfaces are close to normal. Then, adding the four equations in (A1) results in

$$\begin{aligned}&\left(\frac{\vec{E}^{n+1}-\vec{E}^{n}}{\Delta t}\right)\cdot\hat{n}(\varepsilon_1A_1+\varepsilon_2A_2+\varepsilon_3A_3+\varepsilon_4A_4)\frac{A}{A}\\&\quad+\left(\frac{\vec{E}^{n+1}+\vec{E}^{n}}{2}\right)\cdot\hat{n}(\sigma_1A_1+\sigma_2A_2\\&\quad+\sigma_3A_3+\sigma_4A_4)\frac{A}{A}\\&=\left[\vec{\ell}_1\cdot\vec{H}_1^{n+1/2}+\vec{\ell}_2\cdot\vec{H}_2^{n+1/2}\right.\\&\quad\left.+\vec{\ell}_3\cdot\vec{H}_3^{n+1/2}-\vec{\ell}_4\cdot\vec{H}_4^{n+1/2}\right]\end{aligned} \tag{A4}$$

where, A is the total face area. Subsequently, an average permittivity and conductivity are introduced where

$$\varepsilon_{\text{ave}}=\sum_{i=1}^{N_e}A_i\varepsilon_i\Big/A,\quad\sigma_{\text{ave}}=\sum_{i=1}^{N_e}A_i\sigma_i\Big/A \tag{A5}$$

where N_e is the number of subregions and $A=\sum_{i=1}^{N_e}A_i$.

ACKNOWLEDGMENT

The authors would like to acknowledge Dr. D. Antsos for his design of the Wilkinson power divider, and P. Wamhof for his design of the Gysel power divider. This research was performed in part using the Intel Touchstone Delta System operated by the California Institute of Technology on behalf of the Concurrent Supercomputing Consortium. Access to this facility was provided by the Jet Propulsion Laboratory.

REFERENCES

[1] K. S. Yee, "Numerical solution of initial boundary value problems in isotropic media," *IEEE Trans. Antennas Propagat.*, vol. AP-14, pp. 302–307, May 1966.

[2] D. Sheen, S. Ali, M. Abouzahra, and J. A. Kong, "Application of the three-dimensional finite-difference time-domain method to the analysis of planar microstrip circuits," *IEEE Trans. Microwave Theory Tech.*, vol. 38, pp. 849–856, July 1990.

[3] X. Zhang, J. Fang, K. Mei, and Y. Lui, "Calculations of the dispersive characteristics of microstrips by the time-domain finite difference method," *IEEE Trans. Microwave Theory Tech.*, vol. 36, pp. 263–267, July 1988.

[4] X. Zhang and K. Mei, "Time-domain finite difference approach to the calculation of the frequency-dependent characteristics of microstrip discontinuities," *IEEE Trans. Microwave Theory Tech.*, vol. 36, pp. 1775–1787, July 1988.

[5] W. Sui, D. Christensen, and C. Durney, "Extending the two-dimensional FDTD method to hybrid electromagnetic systems with active and passive lumped elements," *IEEE Trans. Microwave Theory Tech.*, vol. 40, pp. 724–730, Apr. 1992.

[6] R. Holland, "Finite-difference solution of Maxwell's equations in generalized nonorthogonal coordinates," *IEEE Trans. Nucl. Sci.*, vol. NS-30, pp. 4589–4591, 1983.

[7] M. Fusco, M. Smith, and L. Gordon, "A three-dimensional FDTD algorithm in curvilinear coordinates," *IEEE Trans. Antennas Propagat.*, vol. 39, pp. 1463–1471, Oct. 1991.

[8] J.-F. Lee, R. Palandech, and R. Mittra, "Modeling three-dimensional discontinuities in waveguides using nonorthogonal FDTD algorithm," *IEEE Trans. Antennas Propagat.*, vol. 40, pp. 346–352, Feb. 1992.

[9] P. Harms, J.-F. Lee, and R. Mittra, "A study of the nonorthogonal FDTD method versus the conventional FDTD technique for computing resonant frequencies of cylindrical cavities," *IEEE Trans. Microwave Theory Tech.*, vol. 36, pp. 741–746, Apr. 1992.

[10] C. Rappaport and E. Smith, "Anisotropic FDFD computed on conformal meshes," *IEEE Trans. Magn.*, vol. 27, pp. 3848–3851, Sept. 1991.

[11] R. Holland, V. Cable, and L. Wilson, "The FVTD technique for electromagnetic scattering," *IEEE Trans. Electromag. Compat.*, vol. 33, pp. 281–294, Nov. 1991.

[12] N. Madsen and R. Ziolkowski, "A modified finite volume technique for Maxwell's equations," *Electromagn.*, vol. 10, pp. 127–145, Jan. 1990.

[13] N. Madsen, "Divergence preserving discrete surface integral methods for Maxwell's equations using nonorthogonal unstructured grids," *J. Computat. Physics*, vol. 119, no. 1, p. 34–45, Jan. 1995.

[14] S. D. Gedney and F. Lansing, "Full wave analysis of printed microstrip devices using a generalized Yee-algorithm," *1993 IEEE Symp. Antennas Propagat. Proceed.*, Ann Arbor, MI, June 27–July 2, 1993.

[15] R. F. Harrington, *Time Harmonic Electromagnetic Fields*. New York, NY: McGraw-Hill, 1961.

[16] V. Betz and R. Mittra, "Comparison and evaluation of boundary conditions for the absorption of guided waves in a FDTD simulation," *IEEE Microwave Guided Wave Lett.*, vol. 2, pp. 499–501, Dec. 1992.

[17] B. Nour-Omid, A. Raefsky, and G. Lyzenga, "Solving finite element equations on concurrent computers," in *Proc. Symp. Parallel Computation and Their Impact on Mechanics*, Boston, Dec. 13–18, 1987.

[18] S. D. Gedney, "Finite-difference time-domain analysis of microwave circuit devices on high performance vector/parallel computers," *IEEE Trans. Microwave Theory Tech.*, vol. 43, pp. 2510–2514, Oct. 1995.

Stephen D. Gedney received the B.Eng.-Honors degree from McGill University, Montreal, P.Q., in 1985, and the M.S. and Ph.D. degrees in electrical engineering from the University of Illinois, Urbana-Champaign, in 1987 and 1991, respectively.

From 1985 to 1987, he worked for the U.S. Army Corps of Engineers, Champaign, IL, where he was engaged in research in EMP pulse simulation and propagation. Since 1991 he has been an Assistant Professor of Electrical Engineering at the University of Kentucky. His current research interests are in the areas of microwave circuit and antenna design and analysis, the analysis of electrical interconnects of VLSI packages, electromagnetic scattering, and the development of parallel computational methods for the analysis of large scale electromagnetic problems.

In 1992 and 1993, Dr. Gedney received the NASA/ASEE Summer Faculty Fellowship at the Jet Propulsion Laboratory, Pasadena, CA, where he was involved in the development of techniques for the full-wave analysis of printed microwave circuits and antennas. He also received the NSF Research Initiation Award in 1993.

Faiza S. Lansing received the B.Sc. degree from Cairo University, Giza, Egypt in 1970, the M.Sc. degree from Syracuse University, Syracuse, in 1976, and the Ph.D. degree from the University of Southern California (USC), Los Angeles, in 1981. She completed her postdoctoral studies at USC in 1982.

From 1970 to 1983, she combined a career in industry and academia. Since 1983, she has been with the Jet Propulsion Laboratory, of California Institute of Technology in Pasadena, CA. where she held several management positions. Currently she is with the Spacecraft Telecommunication Equipment Section as a Member of technical staff implementing advanced techniques for the Project Design Center and the Telecommunications and Data Acquisition Ka-band transmit/receive tasks. Her current research interests are in the areas of electromagnetic modeling of RF circuits and antennas, and visualization.

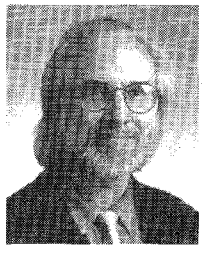

Daniel L. Rascoe received the B.S. degree in physics and mathematics with high honors from Southern Methodist University, the M.S. and Ph.D. degrees in physics from the University of Illinois at Urbana-Champaign, in 1970, 1972, and 1978, respectively. His research thesis was on transmission of phonons in liquid helium under pressure.

From 1978 to 1986 he was with Hughes Aircraft Company, Space and Communications Group functioning in capacities ranging from Group Leader to Section Head and Department Manager. His work involved low noise amplifiers, receivers from 2–20 GHz. Since 1986, he has been with the Jet Propulsion Laboratory where he designed and developed a 21–element, 32–GHz phased array transmit antenna feed utilizing GaAs monolithic microwave integrated circuits (MMIC's) and silicon control IC's. From 1991 to present, he has been the Spacecraft Communications Technology and Advanced Concepts Group supervisor. His interests include electromagnetic modeling of mm wave packaging, design of low noise and high power 32 GHz amplifiers, high temperature superconductor comm applications, and phased array technology.

Dr. Rascoe is a member of Phi Beta Kappa and Sigma Xi.